Normal coordinate analysis, molecular structure, vibrational, electronic spectra and NMR investigation of 4-Amino-3-phenyl-1H-1,2,4-triazole-5(4H)-thione by ab initio HF and DFT me...

ARTICLE *in* SPECTROCHIMICA ACTA PART A MOLECULAR AND BIOMOLECULAR SPECTROSCOPY · AUGUST 2014

Impact Factor: 2.35 · DOI: 10.1016/j.saa.2014.05.081 · Source: PubMed

2 AUTHORS, INCLUDING:

Khaled Bahgat
Suez Canal University
10 PUBLICATIONS **42** CITATIONS

SEE PROFILE

Spectrochimica Acta Part A: Molecular and Biomolecular Spectroscopy 135 (2015) 1145–1155

Contents lists available at ScienceDirect

Spectrochimica Acta Part A: Molecular and Biomolecular Spectroscopy

journal homepage: www.elsevier.com/locate/saa

Normal coordinate analysis, molecular structure, vibrational, electronic spectra and NMR investigation of 4-Amino-3-phenyl-1H-1,2,4-triazole-5(4H)-thione by ab initio HF and DFT method

Khaled Bahgat [a,b,*], Safwan Fraihat [b]

[a] Chemistry Department, Faculty of Petroleum and Mining Engineering, Suez University, Suez, Egypt
[b] Chemistry Department, Collage of Science, Al Jouf University, Sakaka, Saudi Arabia

HIGHLIGHTS

- Spectroscopic properties of the title compound were examined by FT-IR, FT-Raman, UV and NMR techniques, HF and DFT methods.
- Geometrical parameters and vibrational frequencies of the studied compound were calculated.
- The complete assignments are performed on the basis of the potential energy distribution (PED).
- Calculated HOMO–LUMO energy gap is (4.717 eV) at B3LYP/6-311++G(d,p).
- NLO and NBO analysis of the molecule were studied.

GRAPHICAL ABSTRACT

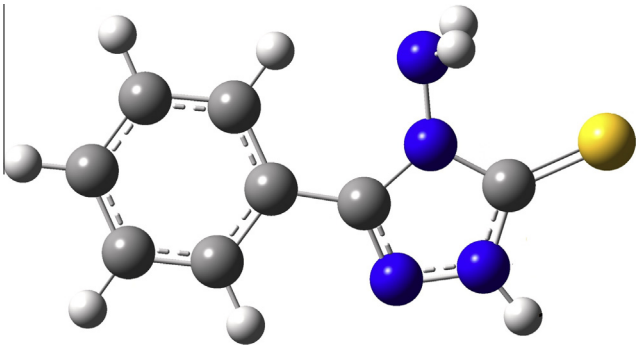

ARTICLE INFO

Article history:
Received 17 March 2014
Received in revised form 26 May 2014
Accepted 30 May 2014
Available online 12 August 2014

Keywords:
4-Amino-3-phenyl-1H-1,2,4-triazole-5(4H)-thione
Vibrational assignments
Normal coordinate analysis
Quantum mechanical calculations

ABSTRACT

In the present work, the characterization of 4-Amino-3-phenyl-1H-1,2,4-triazole-5(4H)-thione (APTT) molecule was carried out by quantum chemical method and vibrational spectral techniques. The FT-IR (4000–400 cm^{-1}) and FT-Raman (4000–100 cm^{-1}) spectra of APTT were recorded in solid phase. The UV–Vis absorption spectrum of the APTT was recorded in the range of 200–400 nm. The molecular geometry, harmonic vibrational frequencies and bonding features of APTT in the ground state have been calculated by HF and DFT methods using 6-311++G(d,p) basis set. The complete vibrational frequency assignments were made by normal coordinate analysis (NCA) following the scaled quantum mechanical force field methodology (SQMF). The molecular stability and bond strength were investigated by applying the natural bond orbital analysis (NBO) and natural localized molecular orbital (NLMO) analysis. The electronic properties, such as excitation energies, absorption wavelength, HOMO and LUMO energies were performed by time depended DFT (TD-DFT) approach. The ^{1}H and ^{13}C nuclear magnetic resonance chemical shift of the molecule were calculated using the gauge-including atomic orbital (GIAO) method and compared with experimental results. Finally, the calculation results were analyzed to simulate infrared, FT-Raman and UV spectra of the title compound which shows better agreement with observed spectra.

Introduction

Traizole are an important class of heterocyclic compounds. Literature reports reveal that many synthetic triazole derivatives

* Corresponding author at: Chemistry Department, Faculty of Petroleum and Mining Engineering, Suez University, Suez, Egypt.

http://dx.doi.org/10.1016/j.saa.2014.05.081
1386-1425/

possesses interesting biological properties [1–7]. Triazole derivatives are also used in the synthesis of antibiotics, fungicides, herbicides, plant growth hormone insulators [8] and potentially good corrosion inhibitions [9,10]. In addition there are some studies on electronic structures and thiol-thione tautomeric equilibrium of heterocyclic thione derivatives [11,12]. 1,2,4-Triazole are very useful ligands in coordination chemistry. The utilization of the 1,2,4-Triazole moiety as a part of ligand system in metal complexes has gained considerable attention in recent years [13,14]. The application of triazole ligand lies in medical research complex with Pt(II) [15] exhibit antitumor activity (human cancer) similar to *Cisplatin*. Vibrational spectroscopy is one of the most widely used methods in spectroscopy and it has proven to be a powerful technique in the determination of the structural properties of various optically active compounds. The molecular modeling studies on pyrazoles are still limited. Molecular modeling was utilized beside FT-IR and FT-Raman spectra for studying the molecular structure of many systems and structures. The structure of 4-benzyl-3-(2-hydroxyphenyl)-1H-1,2,4-triazole-5(4H)-thione in gas phase and in a solid state has been investigated by Koparir et al. [16]. The molecular structure and chemical shift of 3-(2-Hydroxyphenyl)-4-phenyl-1*H*-1,2,4-triazole-5-(4*H*)-thione have been studied by Davut Avcı et al. [17]. Recently Karakurt et al., and Cansız et al., have been studied the vibrational spectral properties as well as NMR of 4-allyl-5-(2-hydroxyphenyl)-2,4-dihydro-3H-1,2,4-triazole-3-thione [18] and 4-Allyl-5-pyridin-4-yl-2,4-dihydro-3H-1,2,4-triazole-3-thione [19]. In their studies they have found that N—H stretching vibrational frequencies get decreased due to N—H---S hydrogen bond. Literature survey reveals that so far there is no complete experimental and theoretical study for the title compound. In this present study, a detailed vibrational spectral investigation of 4-Amino-3-phenyl-1H-1,2,4-triazole-5(4H)-thione (APTT, $C_8H_8N_4S$) has been performed using the scaled quantum mechanical (SQM) force field technique based on density functional theory (DFT) and Hartree–Fock (HF) calculations. In addition, the gauge-including atomic orbital(GIAO) ^{13}C and ^{1}H NMR chemical shifts calculations of the title compounds have been carried out by using the B3LYP method with the 6-311++G(d,p) basis set. The molecular stability and bond strength were investigated by applying the natural bond orbital analysis (NBO) and natural localized molecular orbital (NLMO) analysis. UV spectroscopic studies along with HOMO, LUMO analysis had been used to elucidate information regarding charge transfer within the molecule.

Experimental

4-Amino-3-phenyl-1H-1,2,4-triazole-5(4H)-thione was obtained as previously described in the literature [20]. The infrared spectra were recorded with a Nicolet Magna 750 FT-IR spectrometer equipped with a room temperature DTGS detector. The spectra of the solid (in the 4000–400 cm^{-1} spectral region) were recorded in the form of KBr pellets at a 2 cm^{-1} spectral resolution accumulating 128 scans. The Raman spectra were measured with a Nicolet 950 FT-Raman spectrometer equipped with liquid nitrogen cooled Ge detector. An Nd:YAG laser (1064 nm) was used for excitation at 30–150 mW output power at a spectral resolution of 4 cm^{-1}. NMR spectra were recorded on Bruker Avance 300 VT spectrometer operating at 300.07 and 75.4614 Hz for ^{1}H and ^{13}C, respectively. The ^{1}H and ^{13}C chemical shifts were measured in $CDCl_3$ solution and recalculated relative to TMS by adding 3.55 and 67.35 ppm, respectively. The concentration of the sample was 0.5 M. The electronic spectrum of the title compound in Ethanol was recorded by Unicom UV–Vis spectrometer UV2 using 1 cm Stoppard silica cells.

Results and discussion

Molecular geometry

The calculated optimized geometrical parameters are presented in Table 1 in accordance with the atom numbering scheme of the molecule as shown in Fig. 1. The molecular structure of the title compound is non-planar [20], the benzene ring (C6—C1—C7—N11) form dihedral angle 13.7° with 1,2,4-triazole ring. The global minimum energy obtained by HF and DFT structure optimization using 6-311++G(d,p) basis set for the title molecule as −2423473.3944 and −2433845.257 kJ/mol, respectively. From Table 1 it is observed that the C—N bond distance of triazole ring computed by B3LYP are within 3.6% error and those at HF are 1.55% error. The C—C bond length is predicted within 2.35% at B3LYP and within 1.08% error of experimental value at HF. The N—N is predicted within 1.2% error at B3LYP and 3.35% error at HF. However, the benzene ring appears little distorted and angles slightly out of perfect hexagonal structure, the computed C6—C1, C1—C2, C3—C4 are longer and C2—C3, C4—C5, C5—C6 are shorter. This is also evident from the increase in values of the computed bond angles, C1—C2—C3, C4—C5—C6, C6—C1—C2 and decrease in values of the computed C2—C3—C4, C5—C6—C1 bond angles. The crystal structure is stabilized by intermolecular N—H---S hydrogen bond interactions, the presence of C=S plays a major role in hydrogen bonding of the molecule

Table 1
Experimental and optimized geometrical parameters (bond length, bond, angle, dihedral angle) of 4-Amino-3-phenyl-1H-1,2,4-triazole-5(4H)-thione obtained by B3LYP and HF methods.

Structural parameters	B3LYP	HF	Experimental[a] values
	6-311++G(d,p)	6-311++G(d,p)	
Bond distance (Å)			
C1—C2	1.413	1.386	1.387
C2—C3	1.402	1.384	1.397
C3—C4	1.402	1.382	1.394
C4—C5	1.405	1.383	1.38
C5—C6	1.398	1.383	1.386
C6—C1	1.416	1.379	1.39
C1—C7	1.476	1.388	1.476
C7—C8	1.403	1.475	1.366
N8—C9	1.408	1.377	1.378
C9—N10	1.369	1.356	1.326
N10—N11	1.382	1.32	1.379
C9—S13	1.667	1.666	1.675
N8—N12	1.416	1.381	1.409
N12—H20	1.028	0.998	0.89
N12—H21	1.029	0.998	0.89
N10—H19	1.015	0.989	0.89
Bond angle (°)			
C1—C2—C3	120.1	119.9	119.6
C2—C3—C4	120.6	120.6	121.5
C3—C4—C5	199.6	119.5	119.8
C4—C5—C6	120.3	120.2	119.8
C5—C6—C1	120.4	120.4	120.8
C6—C1—C7	119	119.4	118.5
C1—C7—C8	127.9	128.2	128
C7—C8—C9	109.4	109.7	109.7
N8—C9—N10	101.5	101.7	102.8
N11—N10—C9	114.6	114.5	114.1
N10—N11—C7	104.9	105	104.1
N8—C9—S13	127.7	127.3	125.9
C7—N8—N12	127	127.3	126.7
N8—N12—H20	107.2	106.6	109.3
N8—N12—H21	105.7	106.1	109.3
C9—N10—H19	125.3	125.2	123.6
C6—C1—C7—N11	16.9	8.5	13.7

For numbering of atoms refer Fig. 1.
[a] Values are taken from Ref. [20].

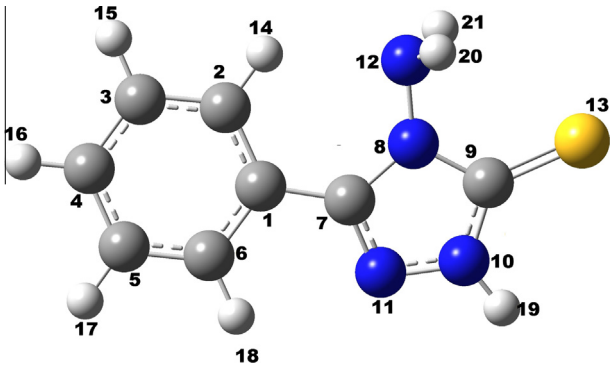

Fig. 1. Molecular structures of 4-Amino-3-phenyl-1H-1,2,4-triazole-5(4H)-thione along with numbering of atom.

(N—H---S) [21]. According to our calculations, C=S bond length is in excellent agreement with the experimental value for both HF and B3LYP methods, indicating the electron density of the lone pairs over the S13 atom is delocalized towards the triazole ring, due to the presence of nitrogen atoms in the ring.

Computational details

The density functional theory B3LYP and RHF at the 6-311++G(d,p) basis set level was adopted to calculate the properties, such as optimized geometries and vibrational frequencies, of the title molecule in this work. All the calculations were performed using Gaussian 03 W program package [22] with the default convergence criteria without any constraint on the geometry [23]. The NMR isotropic shielding constants were calculated using the standard GIAO (Gauge-Independent Atomic orbital) approach [24,25] of the Gaussian 03 package. The electronic properties, such as absorption wavelengths, excitation energies and oscillator strengths were calculated using B3LYP method of the time-dependent DFT (TD-DFT) [26], based on the optimized structure. The prediction of Raman intensities is carried out by following the procedure outlined below. The Raman activities (I_i) calculated by the GAUSSIAN-03 program are adjusted during scaling procedure with MOLVIB and are converted to relative Raman intensities (I_i) using the following relationship derived from the basic theory of Raman scattering [27,28].

$$I_i = \frac{f(v_0 - v_i)^4 S_i}{v_i\left[1 - \exp\left(-\frac{hcv_i}{kT}\right)\right]}$$

where v_0 is the exciting frequency (in cm^{-1} units), v_i is the vibrational wave number of the ith normal mode, h, c, k are the fundamental constants and f is a suitably chosen common normalization factor for all peak intensities.

Normal coordinate analysis

The Gaussian program was used to obtain the vibrational frequencies of the APTT from analytically calculated force constants. The Cartesian force constants were computed at optimized geometry by assuming C1 point group symmetry. Scaling of the force field was performed according to the SQM procedure [29,30] using selective scaling in local symmetry coordinates [31,32]. Transformations of force field and the subsequent normal coordinate analysis including calculation of the potential energy distribution (PED), and the predictions of IR intensity were done using the MOLVIB Program [33]. The full set of 79 standard internal coordinates (containing 22 redundancies) for APTT is defined. From these, a non-redundant set of local symmetry coordinates were constructed by suitable linear combinations of internal coordinates following the recommendations of Fogarasi and Pulay [31,32] as given in Table 2. The theoretically calculated DFT force fields were transformed to this latter set of vibrational coordinates and used in all subsequent calculations. The detailed vibrational assignments of fundamental modes of APTT along with the calculated IR intensity and normal mode descriptions (characterized by PED) are reported in Table 3. For the plots of simulated IR and Raman spectra, pure Lorentzian band shapes are used with a band width (FWHM) of 10 cm^{-1}. The observed and simulated FT-IR and FT-Raman Spectra of APTT are presented in Figs. 2 and 3. The RMS errors of the frequencies (scaled/unscaled) observed for 4-Amino-3-phenyl-1H-1,2,4-triazole-5(4H)-thione are found to be 64.61 and 112.01 cm^{-1} for DFT and HF, respectively. Large deviations were obtained from the vibrations of NH stretch, NH_2 stretch, CS stretch and NH bending due to the large effect of N—H---S hydrogen bond. In order to reproduce the observed frequencies, the scale factors were optimized via least square refinement which resulted a weighted RMS deviation of 11.2 and 25.3 cm^{-1} for DFT and HF, respectively, between the experimental and SQM frequencies. The newly obtained scale factors are given in Table 2. The calculated frequencies by HF are slightly higher than the observed values for the majority of normal modes, so they will not be considered in the further calculations.

N—H vibrations

Heteroaromatic molecules containing an N—H group show it is stretching absorption in the region 3500–3220 cm^{-1} [34]. For substituted triazole N—H stretching mode observed at 3383 cm^{-1} [35] and 3417 [36] as experimentally. Primary amines examined in dilute solution display two weak absorption bands, one near 3500 cm^{-1} and the other near 3400 cm^{-1}. These bands represent, respectively, the asymmetrical and symmetrical N—H stretching modes [37]. In the present work, the FT-IR medium band observed at 3442 cm^{-1} in APTT has been assigned to N—H stretching vibrations. The theoretical calculation indicates the scaled frequency value at 3435 cm^{-1} by B3LYP method gives an excellent agreement with experimental observation. The PED of this mode shows that they are pure stretching mode. The N—H deformation vibration calculated at 1310 cm^{-1} also exactly coincides with experimental observations at 1317 cm^{-1} as a strong FT-IR band, and the same vibration in FT-Raman at 1315 cm^{-1}. The frequency in the FT-IR spectrum at 694 $cm^{-1}$and in FT-IR spectrum at 698 cm^{-1} in the FT-Raman are assigned to NH wagging mode correlates with the frequencies 699 cm^{-1}computed by the B3LYP method.

NH_2 vibrations

The NH_2 group gives rise to six internal modes of vibrations viz., the symmetric stretching, the anti-symmetric stretching, the symmetric deformation or the scissoring, the rocking, the wagging and torsional modes. The NH_2 group has two NH stretching vibrations, one being anti-symmetric and the other symmetric. The frequency of asymmetric vibration is higher than that of symmetric one. In the case of two NH bonds of the NH_2 group being identical, the ν_{as} and ν_s modes satisfy the relationship $\nu_s = 345.5 + 0.876\nu_{as}$ as proposed empirically by Ballamy and Williams [38], where ν_{as} and ν_s are in wavenumbers. For APTT, the two NH_2 stretching modes appear at 3331 and 3253 cm^{-1} in the infrared spectrum. The lower frequency is assigned to the symmetric (ν_s) and the higher one to the anti-symmetric (ν_{as}) mode. Using the relation of Bellamy and Williams and taking ν_{as} to be 3331 cm^{-1}, ν_s comes out to be 3263 cm^{-1} which is 10 cm^{-1} higher than the observed frequency (3253 cm^{-1}). It appears that the two NH bonds of NH_2 group are not equivalent. In addition, the NH_2 group has scissoring (βNH_2), rocking (ρNH_2), wagging (ωNH_2) and torsion (τNH_2)

Table 2
Definition of local-symmetry coordinates.

Symmetry coordinate	Definition	Scale factors by B3LYP/6-311++G(d,p)	Symbol
S_1	r_1	0.86	νNH
S_2	$(r_2 + r_3)/\sqrt{2}$	0.86	νNH_2ss
S_3	$(r_2 - r_3)/\sqrt{2}$	0.86	νNH_2ass
S_{4-8}	r_4, r_5, r_6, r_7, r_8	0.91	νCH
S_{9-14}	r_9, r_{10}, r_{11}, r_{12}, r_{13}, r_{14}	0.922	νC═C
S_{15-18}	r_{15}, r_{16}, r_{17}, r_{18}	0.922	νCN
S_{19}	r_{19}	0.92	νNN
S_{20}	r_{20}	0.91	$\nu N{-}NH_2$
S_{21}	R_{21}	0.922	νC1—C7
S_{22}	R_{22}	0.92	νCS
S_{23-27}	$(\beta_{1,2,14}-\beta_{3,2,14})/\sqrt{2}$, $(\beta_{2,3,15}-\beta_{4,3,15})/\sqrt{2}$, $(\beta_{3,4,16}-\beta_{5,4,16})/\sqrt{2}$, $(\beta_{4,5,17}-\beta_{6,5,17})/\sqrt{2}$, $(\beta_{5,6,18}-\beta_{1,6,18})/\sqrt{2}$	0.95	βCH
S_{28}	$(\beta_{8,12,20}-\beta_{8,12,21})/\sqrt{2}$	0.88	ρNH_2
S_{29}	$(2\beta_{20,8,21}-\beta_{8,12,20}, \beta_{8,12,21})/\sqrt{6}$	0.88	βNH_2
S_{30}	$(\beta_{9,8,12}-\beta_{7,8,12})/\sqrt{2}$	0.922	$\beta N{-}NH_2$
S_{31}	$(\beta_{11,10,19}-\beta_{7,10,19})/\sqrt{2}$	0.95	βN—H
S_{32-33}	$(\beta_{7,1,6}-\beta_{7,1,2})/\sqrt{2}$, $(\beta_{1,7,10}-\beta_{1,7,8})/\sqrt{2}$	0.967	βCC
S_{34}	$(\beta_{11,9,13}-\beta_{8,9,13})/\sqrt{2}$	0.95	βCS
S_{35}	$\beta_{10,7,8} + a\,(\beta_{7,10,11} + \beta_{11,9,8}) + b\,(\beta_{10,11,9} + \beta_{9,8,7})$	0.99	βR_1 (triazol)
S_{36}	$(a-b)\,(\beta_{7,10,11}-\beta_{11,9,8}) + (1-a)\,(\beta_{10,11,9}-\beta_{9,8,7})$	0.99	βR_1 (triazol)
S_{37}	$(\beta_{1,2,3}-\beta_{2,3,4} + \beta_{3,4,5}-\beta_{4,5,6} + \beta_{5,6,1}-\beta_{6,1,2})/\sqrt{6}$	0.99	βCC (R_2 trigid)
S_{38}	$(\beta_{1,2,3}-\beta_{3,4,5} + \beta_{4,5,6}-\beta_{6,1,2})/2$	0.99	βCC (R_2 asymd)
S_{39}	$(-\beta_{1,2,3}-\beta_{2,3,4} + 2\beta_{3,4,5}-\beta_{4,5,6}-\beta_{5,6,1} + 2\beta_{6,1,2})/\sqrt{12}$	0.99	βCC (R_2 symd)
S_{40}	$\omega_{14,2,1,3}$	0.976	ωCH
S_{41}	$\omega_{15,3,2,4}$	0.976	ωCH
S_{42}	$\omega_{16,4,3,5}$	0.976	ωCH
S_{43}	$\omega_{17,5,4,6}$	0.976	ωCH
S_{44}	$\omega_{18,6,1,5}$	0.976	ωCH
S_{45}	$\omega_{12,8,7,9}$	0.976	$\omega N{-}NH_2$
S_{46}	$\omega_{8,12,20,21}$	0.976	ωNH_2
S_{47}	$\omega_{13,9,8,11}$	0.976	ωCS
S_{48}	$\omega_{19,10,7,11}$	0.806	ωN—H
S_{49}	$\omega_{1,7,8,10}$	0.976	ωC1C7
S_{50}	$\omega_{7,1,2,6}$	0.976	ωC7C1
S_{51}	$\tau_{8,7,11,10} + b\,(\tau_{7,11,10,9} + \tau_{10,9,8,7}) + a\,(\tau_{11,10,9,8} + \tau_{9,8,7,11})$	0.935	τR_1(triazol)
S_{52}	$(a-b)\,(\tau_{7,11,10,9}-\tau_{10,9,8,7}) + (1-a)\,(\tau_{11,10,9,8} + \tau_{9,8,7,11})$	0.935	τR_1(triazol)
S_{53}	$(\tau_{1,2,3,4}-\tau_{2,3,4,5} + \tau_{3,4,5,6}-\tau_{4,5,6,1} + \tau_{5,6,1,2}-\tau_{6,1,2,3})/\sqrt{6}$	0.831	τCC (R_2 trigid)
S_{54}	$(\tau_{1,2,3,4}-\tau_{3,4,5,6} + \tau_{4,5,6,1}-\tau_{6,1,2,3})/\sqrt{2}$	0.831	τCC (R_2 asymd)
S_{55}	$(\tau_{1,2,3,4} + 2\tau_{2,3,4,5}-\tau_{3,4,5,6} + \tau_{4,5,6,1} + 2\tau_{5,6,1,2}-\tau_{6,1,2,3})/\sqrt{12}$	0.831	τCC (R_2 symd)
S_{56}	$\tau_{1,12,8,10}$	0.831	$\tau N{-}NH_2$
S_{57}	$\tau_{1,7,8,11}$	0.831	τC1C7

Definitions are made in terms of the standard valence coordinates: r_{ij} is the bond length between atoms i and j; β_{ijk} is the angle between atoms i, j and k; ω_{ijkl} is the out-of-plane angle between the i–j bond and the plane defined by the j, k and l atoms; τ_{ijkl} is the dihedral angle between the planes defined by the i, j, k and j, k, l atoms. ν-stretching, β-in-plane bending, ω-out-of-plane bending, ρ-rocking, τ-torsional. For numbering of atoms, refer Fig. 1. a = cos 144°; b = cos 72°.

modes. The NH_2 scissoring and rocking frequency modes appear in the region of 1700–1600 cm^{-1} and 1150–900 cm^{-1} respectively for amino group [39]. The deformation vibration observed in the FT-IR spectrum as a very strong band at 1631 cm^{-1} is assigned to NH_2 scissoring vibration. The theoretically scaled down value at 1631 cm^{-1} assigned to NH_2 scissoring vibrations are well within the region [40]. The frequency in the FT-IR spectrum at 1297 cm^{-1} is assigned to NH_2 rocking vibration. According to PED this band shows significant coupling with C═N stretching and NH_2 bending. The NH_2 wagging mode (ν_{28}) was assigned to the observed Raman band at 1016 cm^{-1}. The NH_2 torsion vibration computed at 220 cm^{-1} shows good agreement with the recorded FT-Raman frequency of 217 cm^{-1}.

C—N and C═N vibrations

Primary aromatic amine with nitrogen directly on the ring absorb strongly at 1330–1260 cm^{-1} due to stretching of the phenyl carbon—nitrogen bond [41]. In benzotrizole, the C—N stretching band is found to be present at 1382 and 1307 cm^{-1}. The frequencies 1411–1598 cm^{-1} in both FT-IR and FT-Raman spectra have been assigned to C—N, C═N stretching vibration, respectively [42,43]. For 2-mercaptotriazole the C—N and C═N stretching modes were found to be present at 1476, 1573 and 1294 cm^{-1} in FT-IR spectrum have been assigned to C═N and C—N stretching vibrations, respectively [43,44]. In accordance with the above conclusion, for our title molecule the strong to medium absorption bands at 1450 and 1399 cm^{-1} in FT-IR spectrum and at 1448 and 1401 in FT-Raman have been assigned to C═N stretching. Theoretically computed values of C═N vibration falls in the region 1462, 1399 cm^{-1} (mode Nos. 14 and 16). The both experimental and theoretical frequencies of C═N values show in agreement with the literature [44,45]. The FT-IR band observed at 1259 cm^{-1} are assigned to C—N stretching. The counterpart vibrations in FT-Raman spectrum were not observed. The theoretically predicated value at 1252 cm^{-1} exactly correlates with measured experimental data. The other theoretically calculated CNC vibrations such as in-plane-bending and out-of-plane bending vibrations of CNC are also in agreement with experimental observations.

C—H vibrations

The aromatic ring structure shows the presence of C—H stretching vibrations in the region 3100–3000 cm^{-1}, which is the characteristic region of C—H stretching vibrations [46]. The wavenumbers computed in the region 3099–3051 cm^{-1} is assigned to C—H

Table 3
Detailed assignments of fundamental vibrations of 4-Amino-3-phenyl-1H-1,2,4-triazole-5(4H)-thione by normal mode analysis based on SQM force field calculations using B3LYP/6-311++G(d,p).

No.	FTIR observed frequencies (cm^{-1})	FT-Raman observed frequencies (cm^{-1})	Calculated frequencies (cm^{-1})		IR intensity (kM mol^{-1})	Raman intensity (Å amu^{-1})	PED (⩾10%)[a]
			Unscaled	Scaled			
υ_1	3442m	–	3666	3435	118.50	5.09	υNH(98)
υ_2	3331m	–	3508	3344	12.37	2.02	υNH_{2as}(80), NH_{2s}(16)
υ_3	3253m	–	3447	3257	14.58	4.25	υNH_{2s}(93)
υ_4	–	–	3231	3107	3.82	2.66	υCH(99)
υ_5	3095w	–	3204	3084	3.44	4.66	υCH(100)
ν_6	–	–	3189	3065	18.08	12.7	υCH(99)
ν_7	–	3057w	3177	3054	12.98	6.53	υCH(100)
ν_8	3046w	3051w	3167	3044	0.02	3.01	υCH(99)
ν_9	1631vs	1598m	1705	1631	54.87	55.5	βNH_2(62), ρNH2(24)
ν_{10}	1579s	1581s	1643	1578	0.19	22.1	υC=C(43), βCH(33)
ν_{11}	1534s	1533m	1622	1526	2.01	31.2	υC=C(46), υCN(21)
ν_{12}	1508s	1502m	1574	1496	49.14	2.88	υC=C(46), βCH(44)
ν_{13}	1483m	1481s	1526	1476	59.76	14.0	υC=C(51), υC1C7(19), βNNH_2(10)
ν_{14}	1450m	1448s	1493	1462	340.85	45.9	υCN(29), βNNH_2(26), βCH(11)
ν_{15}	1417m	1411w	1477	1428	2.95	64.3	υC=C(37), βCH (14), υCN(14)
ν_{16}	1399m	1401w	1441	1399	17.63	4.53	υCN(40), βCH(18), βNNH_2(12), υC=C(12)
ν_{17}	1317vs	1315s	1369	1310	16.74	0.82	βCH(77), υC=C(10)
ν_{18}	–	–	1358	1307	1.15	4.21	υNN(46), υCN(18), βNH_2(14), ρNH_2(12)
ν_{19}	1297w	1282w	1336	1298	4.12	2.96	ρNH_2(35), υCN(15), βNH_2(13), βNNH_2(11)
ν_{20}	1259m	–	1325	1252	23.26	1.95	υCN(39), υCS(24), υNN(18)
ν_{21}	1228w	1228w	1274	1219	84.38	1.84	βCH(62), υC=C (24)
ν_{22}	1182vw	1180w	1227	1200	31.15	8.40	βCH(53), υC=C (31)
ν_{23}	1163w	1159w	1208	1145	6.91	10.1	βCH(69), υC=C(28)
ν_{24}	1112w	1122w	1185	1124	0.14	5.95	υC=C(54), βCH(44)
ν_{25}	1097w	1091w	1133	1104	8.95	4.48	βCH(63), υCN(11)
ν_{26}	1073s	–	1104	1070	21.16	29.1	νNN(20), βNNH_2(16), νCS(11)
ν_{27}	–	1072m	1096	1051	19.61	1.45	νCN(38), νCS(12), νC1C7(10)
ν_{28}	–	1016w	1053	1012	1.03	0.29	ωNH_2(43), $R2_{trigid}$(20)
ν_{29}	1005s	1001s	1030	1002	60.56	1.50	υC=C(48), R2 $_{trigid}$(27), βCH(23)
ν_{30}	–	983vw	1016	972	2.49	0.53	ωCH(98)
ν_{31}	–	–	1008	953	0.32	0.12	ωCH(68), $\tau R2_{asymd}$(28)
ν_{32}	–	–	997	945	0.44	23.1	υC=C(28), βNH_2(24), νCN(21)
ν_{33}	944vs	–	952	925	48.56	2.30	ωCH(91)
ν_{34}	–	–	950	920	18.13	40.5	υNN(36), βR1(14), υCN(13)
ν_{35}	854vw	–	862	852	0.51	3.17	ωCH(99)
ν_{36}	742m	729m	784	741	25.42	0.82	ωCH(61), ωC7C1(20), ωC1C7(16)
ν_{37}	–	707m	733	709	0.49	14.5	βNNH_2(47), νCN(14), $R2_{symd}$(10)
ν_{38}	694m	698w	714	699	1.93	3.58	ωNH(43), υC1C7(32), τR1(10)
ν_{39}	684m	–	704	690	74.78	2.27	$R2_{symd}$(86), βCH(16)
ν_{40}	–	–	702	667	6.92	0.66	ωNN(50), ωC7C1(30), τR1(10)
ν_{41}	–	–	669	662	6.18	1.52	ωCS(73), τR1(16)
ν_{42}	609w	–	633	618	1.30	5.07	$R2_{asymd}$(65), βCH(23)
ν_{43}	599m	592w	609	594	25.66	4.09	$R2_{trigid}$(66), βCH(18), νCS(15)
ν_{44}	518m	–	535	515	27.07	3.50	ωNH(44), tR1(24), ωC7C1(13)
ν_{45}	503m	505m	518	501	18.57	10.7	βCS(24), βNH(22), νCS(11)
ν_{46}	–	470vs	484	473	24.13	1.25	ωC1C7(54), ωC7C1(26)
ν_{47}	–	–	409	384	0.09	0.637	$\tau R2_{asymd}$(73), ωCH(18)
ν_{48}		332w	348	332	1.20	0.786	ωC1C7(28), ωC7C1(24)
ν_{49}	–	–	321	307	1.93	4.00	ωNH(27), tR1(25), ωC1C7(14)
ν_{50}	–	299w	295	292	5.68	5.85	βC7C1(28), νC1C7(14), βC1C7(11)
ν_{51}	–	279w	262	260	6.70	29.7	ωCS(56), βC1C7(19)
ν_{52}	–	217vs	219	220	8.65	5.75	τNH_2(67), ωCS(9)
ν_{53}	–	162m	177	171	1.71	24.2	τNN(34), τR1(20), ωNN(14)
ν_{54}	–	152vs	164	149	30.33	29.1	τNN(62)
ν_{55}	–	–	153	140	3.16	33.8	βNH (38), βC1C7(26), βCS(15)
ν_{56}	–	–	108	97	1.15	7.52	τC1C7(45), ωC7C1(27), ωNH(10)
ν_{57}	–	–	66	66	0.59	13.5	τC1C7(67), τNN(13)

[a] Potential energy distribution.

stretching vibrations. Herein our present study, the strong broad band observed at 3095 cm^{-1}in the FT-IR and weak bands observed at 3057, 3051 cm^{-1}in the FT-Raman spectrum are assigned to C—H stretching vibrations. The C—H stretching modes, which are not all observed experimentally have been predicted on the basis of PED percentage. The calculated modes 3107, 3084, 3065, 3054 and 3044 cm^{-1} (mode Nos. 4–8) are pure modes, as it is evident from PED column, and they are almost contributing to more than 99%.

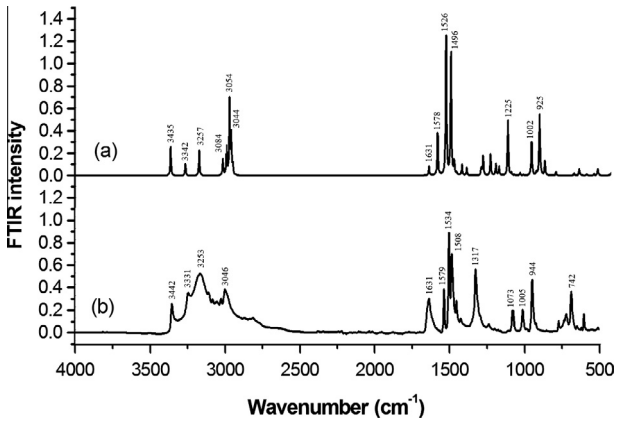

Fig. 2. (a) Simulated B3LYP level FT-IR spectra and (b) experimental FT-IR spectra of APTT.

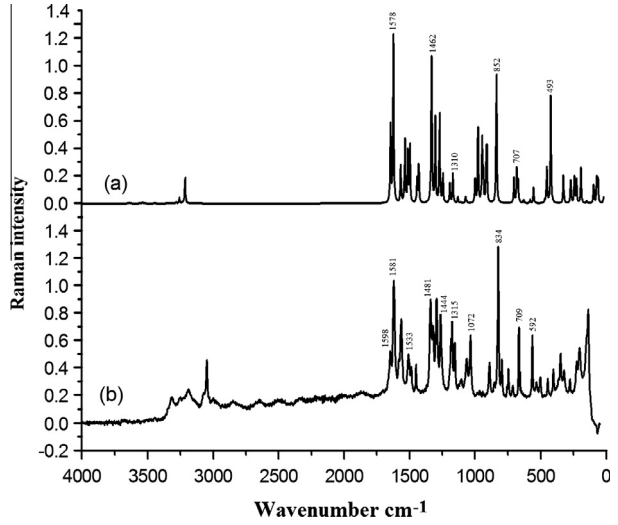

Fig. 3. (a) Simulated B3LYP level FT-Raman spectra and (b) experimental FT-Raman spectra of APTT.

The C—H in-plane ring bending vibrations are normally occurs as a number of strong to weak intensity bands in the region 1000–1300 cm^{-1} [47,48]. In our present study the bands observed in the FT-IR spectrum at 1317, 1228, 1182, 1163 and 1097 cm^{-1} are assigned to C—H in-plane bending vibration and their counter parts in the FT-Raman spectrum are observed at 1315, 1228, 1180, 1159 and 1091 cm^{-1} [49]. The theoretically calculated values 1310, 1219, 1200, 1145 and 1104 cm^{-1} (mode Nos. 17, 21, 22, 23, 25) is in good agreement with the experimental values. The C—H out-of-plane bending vibration is expected in the range 750–1000 cm^{-1} in the FT-IR spectra of substituted benzenes [50,51]. The position of C—H out-of-plane vibration is determined almost extensively by the relative position of the substituents and is independent of nature [52]. The bands observed at 944, 854, 742 cm^{-1} in the FT-IR and 983 cm^{-1} in the FT-Raman spectra are assigned to C—H out-of plane bending vibration.

C—C vibrations

The ring stretching vibrations are very much important in the spectrum of aromatic compounds and are highly characteristic of the aromatic ring itself. However, empirical assignments of vibrational modes for peaks in the finger print region are difficult. Bands between 1400 and 1650 cm^{-1} in benzene derivatives are assigned to these modes. In general, the bands are of variable intensity and observed at 1625–1590, 1590–1575, 1540–1470, 1460–1430 and1380–1280 cm^{-1} from the frequency ranges given by Varsanyi [53] for the five bands in the finger print region. In the present work, the bands width are of different intensity and observed at 1579, 1534, 1508, 1483, 1417 and 1122 cm^{-1} in FT-IR have been assigned to C=C stretching vibrations. The theoretically calculated values at 1578, 1526, 1496, 1476, 1428 and 1124 cm^{-1} agrees well with the experimental values. Only three infrared bands at 684, 609 and 599 cm^{-1} (modes Nos. 39, 42–43) assigned to C—C—C in-plane bending vibrations of APTT. The theoretical calculations indicate the presence of significant mixing of C—C in-plane bending mode and C—H in-plane bending vibrations. All the bands are observed with medium intensities. Their contributions in PED are in the range 50–80%.

C=S vibrations

Identification of C=S stretching vibration is difficult and also uncertain. Since the absorption of C—O and C—N also occur in the same region. C=S group is less polar than the C=O group and has a considerably weak band. In the literature, some C=S stretching modes observed for different substituent-triazole ring are 1166 cm^{-1} [54], 1258 cm^{-1} [43] and 1189 cm^{-1} [19] as experimentally. In this study, the frequencies observed in FT-IR at 1259 cm^{-1} is assigned to C=S mode. The theoretically scaled values at 1252 and 1051 cm^{-1} by B3LYP method exactly correlates with the experimental observations. According to PED this vibration is mixed with other (amino and CN) vibrations, therefore gives only 24–12% contribution to the υ_{20} and υ_{25} fundamental (cf. Table 3). The C=S in-plane bending vibrations obtained as a medium band at 503 cm^{-1} in FT-IR and 505 cm^{-1} in FT-Raman spectra. The theoretically scaled value at 501 cm^{-1} (mode No. 45) agrees well with the experimental values. The C=S out-of-plane bending vibration assigned to 279 cm^{-1} (in FT-Raman band).

NBO/NLMO analysis

Natural bond orbital (NBO) analysis provides an efficient method for studying interesting features of molecular structure. They give strong insight in the intra and inter molecular bonding and interaction among bonds, and also provide a convenient basis for investigation of charge transfer or conjugative interactions in molecular system [55]. Another useful aspect of NBO method is that it gives information about interactions in both filled and virtual orbital spaces that could help to have a detailed analysis of intra and intermolecular interactions. The second order Fock matrix was carried out to evaluate the donor–acceptor interactions in the NBO analysis [56]. For each donor NBO (i) and acceptor NBO (j), the stabilization energy associated with $i \rightarrow j$ delocalization can be estimated as,

$$E(2) = \Delta E_{ij} = q_i = \frac{F(i,j)^2}{\varepsilon_i \varepsilon_j}$$

where q_i is the donor orbital occupancy, ε_i, ε_j are diagonal elements (orbital energies) and $F(i,j)$ is the off-diagonal NBO Fock matrix element. Significant donor–acceptor interactions of APTT and their second order perturbation energies are given in Table 4. The larger the $E(2)$ value, the intense is the interaction between electron donors and electron acceptors. In APTT, the interaction π^* C7—N11 $\rightarrow$ π^* C1—C2 has the highest $E(2)$ value around 62.01 kcal/mol and hence gives the strongest stabilization to the structure. Similarly, the interactions π^* C9—N10 $\rightarrow$ π^* C7—N11 and π C1—C2 $\rightarrow$ π^* C5—C6,

Table 4
Significant donor–acceptor interactions of 4-Amino-3-phenyl-1H-1,2,4-triazole-5(4H)-thione and their second order perturbation energies.

Donor NBO (*i*)	Acceptor NBO (*i*)	*E*(2) (kcal/mol)[a]	*Ej*−*Ei* (a.u)[b]	*F*(*i*,*j*) (a.u)[c]
BD(1) C1—C2	BD*(1) C1—C6	4.65	1.27	0.069
	BD*(1) C2—C3	2.84	1.29	0.054
	BD*(2) C3—C4	18.72	0.29	0.066
	BD*(2) C5—C6	20.06	0.29	0.069
	BD*(2) C7—N11	21.71	0.25	0.067
BD(1) C2—C3	BD*(1) C1—C2	3.36	1.28	0.058
	BD*(1) C1—C7	3.79	1.16	0.059
BD(2) C3—C4	BD*(2) C1—C2	21.90	0.28	0.071
	BD*(2) C5—C6	18.99	0.29	0.067
BD(1) C3—H 15	BD*(1) C1—C2	3.92	1.10	0.059
BD(1) C4—C5	BD*(1) C3—C4	2.78	1.29	0.054
	BD*(1) C5—C6	2.89	1.30	0.055
	BD*(1) C6—H18	2.40	1.17	0.047
BD(1) C4—H16	BD*(1) C2—C3	3.78	1.11	0.058
	BD*(1) C5—C6	3.69	1.12	0.057
BD(2) C5—C6	BD*(2) C1—C2	19.49	0.28	0.067
	BD*(2) C3 -C4	21.04	0.29	0.070
BD(1) C7—N8	BD*(1) C1—C 7	1.51	1.28	0.039
	BD*(1) C9—S13	4.22	1.08	0.060
BD(1) C7—N11	BD*(1) N8—N12	3.68	1.21	0.059
	BD*(1) N10—H19	2.49	1.31	0.051
	BD*(2) C1—C2	7.09	0.38	0.050
	BD*(2) C9—N10	8.27	0.29	0.050
BD(1) N8—C9	BD*(1) C1—C7	3.02	1.31	0.056
	BD*(1) N10—H19	3.76	1.26	0.061
BD(1) C9—N10	BD*(1) N8 – N12	4.89	1.20	0.069
	BD*(2) C7—N11	11.45	0.38	0.062
BD(1) C9—S13	BD*(1) C7—N8	2.84	1.06	0.049
BD(1) N10—N 11	BD*(1) C1—C7	5.14	1.30	0.073
BD*(2) C7—N 11	BD*(2) C1—C2	62.01	0.03	0.069
BD*(2) C 9—N 10	BD*(2) C7—N11	15.31	0.06	0.039
LP(1) N8	BD*(2) C7—N11	42.03	0.29	0.101
	BD*(2) C9—N10	61.25	0.23	0.113
LP(1) N11	BD*(1) C7—N8	5.50	0.82	0.060
LP(1) N12	BD*(1) N8—C9	9.01	0.76	0.075
LP(3) S13	BD*(2) C9—N10	73.04	0.12	0.090

BD = bonding molecular orbital, BD* = antibonding molecular orbital, LP = Lone pair (nonbonding molecular orbital).
[a] *E*(2) means energy of hyperconjucative interactions.
[b] Energy difference between donor and acceptor *i* and *j* NBO orbitals.
[c] F(*i*,*j*) is the Fock matrix element between *i* and *j* NBO orbitals.

π C5—C6 → π* C3—C4 and π C9—N10 → π* C7—N11 are giving stabilization to the structure because of their higher *E*(2) values. The interaction between lone pair N8 with anti bonding C7—N11 and C9—N10, results in a stabilization energy 42.03 and 61.25 kcal/mol which denotes large delocalization. The maximum energy transfer occurs from LP(3) S13 → π* C9—N10 (73.04 kcal/mol) as shown in Table 4. The Natural Localized Molecular Orbital (NLMO) analysis has been carried out since they show how bonding in a molecule is composed from orbitals localized on different atoms. The derivation of NLMOs from NBOs gives direct insight into the nature of the localized molecular orbital's "delocalization tails" [57,58]. Table 5 shows the comparative study of significant NLMO's occupancy, percentage from parent NBO and atomic hybrid contributions of APTT calculated at B3LYP level using 6-311++G(d,p) basis set. In APTT, BD(2) C3—C4 is the most delocalized NLMO having around 81.08% of contribution from the parent NBO. The delocalization tail (~20.11%) consists of the hybrids of C1, C2, C5 and C7. The significant amount of delocalization tail of an NLMO indicates that they are strongly delocalized into the vicinal regions. This delocalization can also be observed in the perturbation theory energy analysis given in Table 4.

Frontier molecular orbital

The frontier orbitals, HOMO and LUMO determine the way how the molecule interacts with other species and helps to characterize the chemical reactivity and kinetic stability of the molecule [59]. They play an important role in the electric and optical properties, as well as in the UV–Vis spectra and chemical reactions. HOMO energy determines the ability to donate an electron and LUMO energy determines the ability to accept an electron. The energy gap between the HOMO and LUMO is very important in determining the chemical reactivity of the molecule. A small HOMO–LUMO energy gap implies low kinetic stability, because it is energetically favorable to add electrons to a low-lying LUMO and to receive electrons from a high-lying HOMO [60]. Thus, molecules with low frontier orbital gap are more polarizable and associated with high chemical reactivity. Fig. 4 shows the distributions HOMO-2, HOMO, LUMO and LUMO + 2 orbital's computed at the B3LYP/6-311++G(d,p) level for the APTT. The calculations indicate that the title compound has (50) occupied molecular orbital. Recently the energy gap between HOMO and the LUMO has been used to prove the bioactivity from intra molecular charge transfer (ICT). Both the HOMO and HOMO-2, electrons are delocalized on the S1 atom and triazole ring. For the LUMO and LUMO + 2 electrons are mainly delocalized on the triazole and benzene rings. The HOMO lying at −5.69 eV (computed by TD-DFT), and the LUMO lying at −1.27 eV HOMO (orbital 50) → LUMO (orbital 51) transition implies an ED transfer to phenyl from the lone pair of sulfur atom (π → π* transition) and from the triazole ring. The energy difference between the HOMO and LUMO was obtained as 4.417 eV in the gas phase calculations. With this large energy gap, it can be

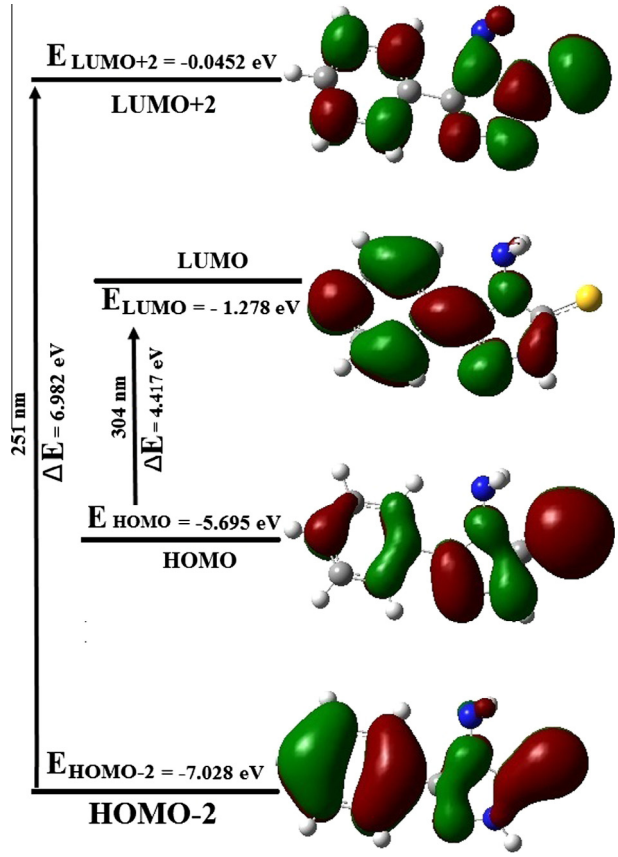

Fig. 4. The atomic orbital compositions of the frontier molecular orbitals for APTT.

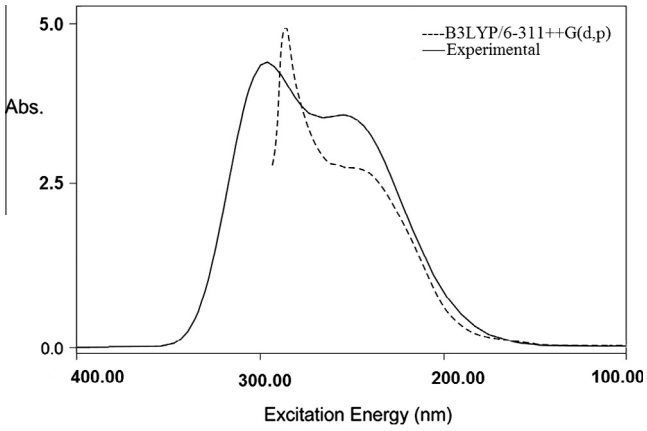

Fig. 5. Experimental and calculated UV–vis spectra of APTT.

said that the title molecule has high kinetic stability and a high chemical hardness.

UV–Vis studies and electronic properties

On the basis of a fully optimized ground-state structure, TD-DFT has been used to determine the low-lying excited states of APTT. The electronic spectra of APTT were computed in the gas phase and the ethanol environments. The solvent effect was calculated using CPCM method. The electronic absorption spectrum of the title compound in ethanol was recorded within the 200–400 nm range and the representative spectrum of computed transitions plot on the experimental is shown in Fig. 5. The computed result shows that the HOMO to LUMO transition corresponds to the λ max absorption band in the UV–Vis spectrum. The calculated results involving the vertical excitation energies (E), oscillator strength (f) and wavelength (λ) are compared with measured experimental wavelengths (Table 6). As can be seen from Fig. 5, electronic absorption spectrum of APTT shows two bands at 251 and 304 nm. From TD-DFT calculation, the most significant theoretical absorption bands are predicted at 249, 282 and 324 nm and can easily be seen that they correspond well with the experimental. The TD-DFT calculation predicts one electronic transition at 324 nm with an oscillator strength f = 0.237, in good agreement with the experimentally measured intense band at 304 nm in ethanol as shown in Fig. 5. This electronic absorption corresponds to the transition from the ground to the first excited state and is mainly described by one electron excitation from the HOMO to the LUMO. The first dipole allows (50 → 51) in the gas phase at 329 nm with oscillation strength of 0.121. From Fig. 5, it is evident that the one narrow shoulder at 251 nm in experimental UV spectrum in ethanol is concerned with the HOMO-2, (orbital 48) → LUMO + 2 (orbital 53) and HOMO (orbital 50) → LUMO + 2 (orbital 53) electronic transitions, in ethanol and gas phase, respectively. The corresponding theoretical peak is found in the TD-DFT UV spectra in ethanol/gas at 249 nm and 258 nm with higher oscillation strength of 0.495 and 0.220 in ethanol and gas phase, respectively.

NMR spectra

B3LYP method with 6-311++G(d,p) basis set was used in order to calculate GIAO ^{1}H and ^{13}C chemical shift values (with respect to TMS), which then compared with the experimental ^{1}H and ^{13}C chemical shift values (as shown in Figs. 6 and 7). Experimental and calculated values for ^{13}C and ^{1}H NMR are shown in Table 7. Taking into account that the range of ^{13}C NMR chemical shift for analogous organic molecules usually is >100 ppm [61,62] the accuracy ensures reliable interpretation of spectroscopic parameters. In the present work, ^{13}C NMR chemical shifts in the ring for the title molecule are >100 ppm, as would be expected (cf. Table 7). We have calculated ^{13}C chemical shift values (with respect to TMS) of 121.59–154.48 ppm with 6-311++G(d,p), while, the experimental results were observed to be 128.57–167.39 ppm. Nitrogen and

Table 6
Experimental and calculated absorption wavelength λ (nm), excitation energies E (eV), oscillator strengths (f) of the most significant singlet excited states for 4-Amino-3-phenyl-1H-1,2,4-triazole-5(4H)-thione. At the B3LYP/6-311++G(d,p) level of theory.

Transition	Experimental λ (nm)	TD-DFT method/ethanol			TD-DFT method/gas phase		
		λ (nm)	Excitation energy E (eV)	Oscillator strength f	λ (nm)	Excitation energy E (eV)	Oscillator strength f
I	304	324	4.07 (50 → 51)	0.237	329	3.82 (50 → 51)	0.121
II	–	282	4.39 (50 → 52)	0.033	280	4.42 (49 → 52)	0.032
III	–	263	4.71 (49 → 52)	0.018	272	4.55 (50 → 52)	0.033
IV	251	249	4.98 (48 → 53)	0.495	258	4.78 (50 → 53)	0.220
V	–	240	5.16 (47 → 51)	0.140	249	4.97 (47 → 51)	0.287

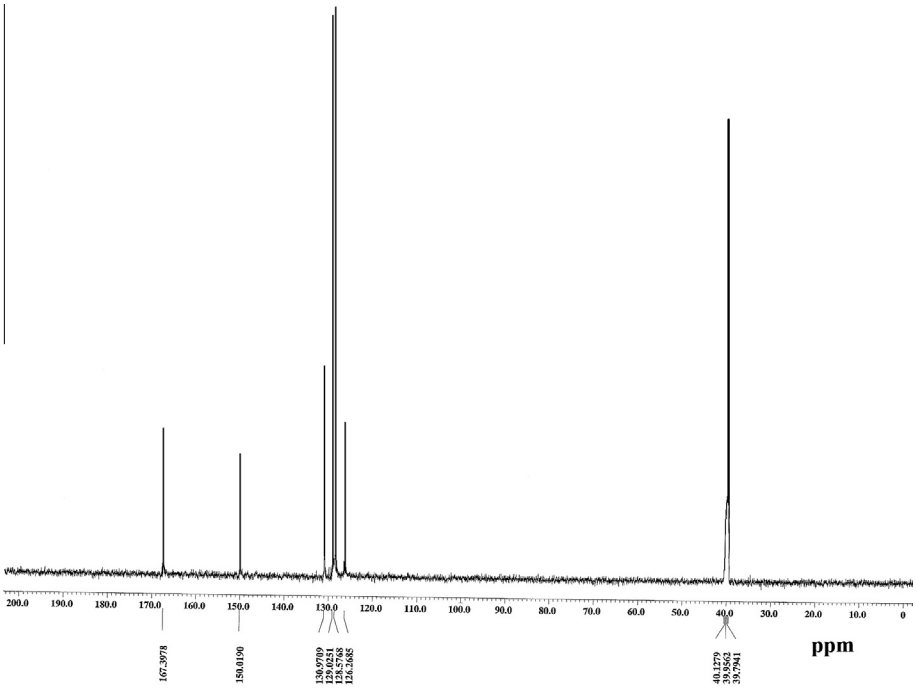

Fig. 6. ^{13}C NMR spectrum of ATTP.

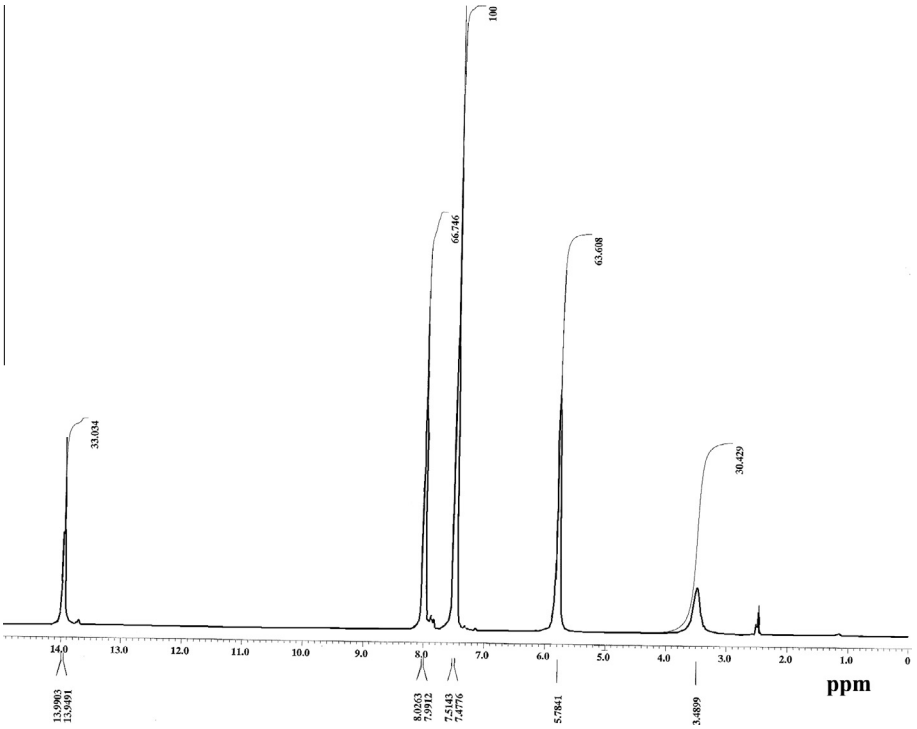

Fig. 7. ^{1}H NMR spectrum of ATTP.

sulfur atoms show electronegative property. Therefore, the chemical shift value of C7 and C9 are higher, 150.02, 167.39 ppm respectively, than the other carbon atoms. Four carbon peaks in the ring that are observed from 128.57 to 130.98 ppm are calculated from 121.59 to 125.08 ppm. Moreover, the pairs C2/C6 as well as C3/C5 are expected to be isochronous due to signal averaging. These results also support our theoretical results as shown in Table 7. We have calculated ^{1}H chemical shift values (with respect to TMS) of 5.06–11.86 ppm at B3LYP/6-311G++(d,p) level, whereas the experimental results are observed to be 5.78–13.99 ppm. The singlet observed at 5.78 ppm is assigned to N(12)H20 and N(12)H21. The aromatic protons resonate at 7.48–8.03 ppm multiplet experimentally, that have been calculated at 6.07–8.92 ppm. In different substituent-1,2,4-triazole, the H chemical shift of N—H was observed to be 11.33–13.56 ppm. The NH hydrogen of the 1,2,4-triazole ring appears at 13.99 ppm, and is determined

Table 7
Theoretical and experimental ^{1}H and ^{13}C isotropic chemical shifts (with respect to TMS, all values in ppm) for the 4-Amino-3-phenyl-1H-1,2,4-triazole-5(4H)-thione.

Atom	Experimental (ppm) (DMS-d_6)	Calculated (ppm) B3LYP/6-311++G(d,p)
C1	128.57	121.59
C2	130.98	122.48
C3	129.03	124.31
C4	126.27	125.08
C5	129.03	124.31
C6	130.98	122.48
C7	150.02	146.66
C9	167.39	154.48
H14	7.99	6.86
H15	7.52	6.75
H16	7.48	6.07
H17	7.51	6.98
H18	8.03	8.92
H19	13.99	11.86
H20	5.78	5.15
H21	5.78	5.06

computationally at 11.86 ppm. Because the intermolecular hydrogen bonds in molecular structure of APTT are neglected in the calculations, we can say that this difference between experimental and calculated chemical shifts is due to N—H---S intramolecular interactions.

Conclusion

FT-IR and FT-Raman spectral measurements and ab inito/DFT calculations have been reported for APTT. A complete vibrational assignment has been proposed on the basis of normal coordinate analysis, electronic structure calculations and potential energy distributions of normal modes. The calculation of the PEDs in terms of local-symmetry coordinates permitted an easy assignment of most of the normal modes. There is a good agreement between computed optimized parameters (i.e., bond lengths and bond angles), and the vibrational frequencies and experimental results. The theoretical UV spectrum is in good agreement with the experimental data. The chemical shifts were compared with experimental data in DMSO solution, showing a very good agreement both for ^{13}C and ^{1}H chemical shifts. The stability and intramolecular interactions have been interpreted by NBO/NLMO analysis and the transactions give stabilization to the structure have been identified by second order perturbation energy calculations.

Acknowledgments

The authors are very thankful to Prof. Tom Sundius, Faculty of Science, Department of Physics, University of Helsinki for valuable suggestions and timely help to carry out this work successfully.

Appendix A. Supplementary material

Supplementary data associated with this article can be found, in the online version, at http://dx.doi.org/10.1016/j.saa.2014.05.081.

References

[1] S. Cansiz, M. Servi, M. Koparir, M. Altintas, J. Digrak, Chem. Soc. Pakistan 23 (2001) 237–240.
[2] M.D. Mullicon, M.W. Wilson, D.T. Connor, C.R. Kostlan, D.J. Schrier, R.D. Dyer, J. Med. Chem. 36 (1993) 1090–1099.
[3] Desai, A.J. Baxi, Indian J. Pharm. Sci. 54 (1992) 183–188.
[4] S.A. Shans El-Dine, A.A.B. Hazzaa, Pharmazie 29 (1974) 761–763.
[5] J.K. Sugden, T. Yoloye, Pharm. Acta Helv. 53 (1978) 65–92.
[6] P.C. Unangst, G.P. Shurum, D.T. Connor, R.D. Dyer, D.J. Schrier, J. Med. Chem. 35 (1992) 3691–3698.
[7] W. Li, Q. Wu, Y. Ye, M. Luo, L. Hu, Y. Gu, F. Niu, J. Hu, Spectrochim. Acta A60 (2004) 2343–2354.
[8] B. Mernari, H. Elattari, M. Triasnel, F. Bentiss, M. Langrenee, Corros. Sci. 40 (1998) 391–399.
[9] F. Bentiss, M. Langrenes, M. Traisnel, J.C. Hornez, Corros. Sci. 41 (1999) 789–803.
[10] N. Dege, A. Cetin, A. Cansiz, M. Sekerci, C. Kazaz, M. Dincer, O. Buyukgungor, Acta Cryst. E60 (2004) o1883–o1885.
[11] M.H. Klingele, S. Brooker, Coord. Chem. Rev. 241 (2003) 119–132.
[12] S. Ozturk, M. Akkurt, A. Casiz, M. Koparir, M. Sekerci, F.W. Heinemann, Acta Cryst. E60 (2004) 0642.
[13] U. Beckmann, S. Brooker, Coord. Chem. Rev. 245 (2003) 17–29.
[14] R.N. Muller, L.V. Elst, S. Laurent, J. Am. Chem. Soc. 125 (2003) 8405–8407.
[15] S. Komeda, S. Bombard, S. Perrier, J. Reedijk, J. Kozelka, J. Inorg. Biochem. 96 (2003) 357–366.
[16] Metin Koparir, Cahit Orek, Naci Ömer Alayunt, Akif Evren Parlak, Pelin Koparir, Kamiran Sarac, Sevgi Durna Dastan, Nevin Cankaya, Commun. Comput. Chem. 1 (2013) 244–268.
[17] Davut Avcı, Yusuf Atalaya, S. Mehmet, Ekercib, Muharrem Dincer, Spectrochim. Acta A 73 (2009) 212–217.
[18] Tuncay Karakurta, Muharrem Dinc, Era, C. Ahmet, Etinb, S. Memet, Ekerci, Spectrochim. Acta A77 (2010) 189–198.
[19] A. Cansıza, C. Oreka, M. Koparira, P. Koparirb, A. Cetin, Spectrochim. Acta Part A 91 (2012) 136–145.
[20] Hong-Yan Wang, Pu-Su Zhao, Rong-Qing Li, Su-Min Zhou, Molecules 14 (2009) 608–620.
[21] S. Gunasekaran, S.R. Varadhan, K. Manoharan, Asian J. Phys. 2 (3) (1993) 165.
[22] M.J. Frisch, G.W. Trucks, H.B. Schlegel, G.E. Scuseria, M.A. Robb, J.R. Cheeseman, J.A. Montgomery, Jr., T. Vreven, K.N. Kudin, J.C. Burant, J.M. Millam, S.S. Iyengar, J. Tomasi, V. Barone, B. Mennucci, M. Cossi, G. Scalmani, N. Rega, G.A. Petersson, H. Nakatsuji, M. Hada, M. Ehara, K. Toyota, R. Fukuda, J. Hasegawa, M. Ishida, T. Nakajima, Y. Honda, O. Kitao, H. Nakai, M. Klene, X. Li, J.E. Knox, H.P. Hratchian, J.B. Cross, C. Adamo, J. Jaramillo, R. Gomperts, R.E. Stratmann, O. Yazyev, A.J. Austin, R. Cammi, C. Pomelli, J.W. Ochterski, P.Y. Ayala, K. Morokuma, G.A. Voth, P. Salvador, J.J. Dannenberg, V.G. Zakrzewski, S. Dapprich, A.D. Daniels, M.C. Strain, O. Farkas, D.K. Malick, A.D. Rabuck, K. Raghavachari, J.B. Foresman, J.V. Ortiz, Q. Cui, A.G. Baboul, S. Clifford, J. Cioslowski, B.B. Stefanov, G. Liu, A. Liashenko, P. Piskorz, I. Komaromi, R.L. Martin, D.J. Fox, T. Keith, M.A. Al-Laham, C.Y. Peng, A. Nanayakkara, M. Challacombe, P.M.W. Gill, B. Johnson, W. Chen, M.W. Wong, C. Gonzalez, J.A. Pople, Gaussian 03, Revision B. 03, Gaussian Inc., Pittsburgh, PA, 2003.
[23] H.B. Schlegel, J. Comput. Chem. 3 (1982) 214.
[24] K. Wolinski, K. Hinton, P. Pulay, J. Am. Chem. Soc. 112 (1990) 8251.
[25] B. Ośmialowski, E. Kolehmainen, R. Gawinecki, Magn. Reson.Chem. 39 (2001) 334.
[26] E. Runge, E.K.U. Gross, Phys. Rev. Lett. 52 (1984) 997.
[27] G. Keresztury, Raman spectroscopy: theory, in: J.M. Chalmers, P.R. Griffiths (Eds.), Hand Book of Vibrational Spectroscopy, vol. 1, Wiley, 2002, pp. 71–87.
[28] G. Keresztury, S. Holly, J. Varga, G. Besenyei, A.Y. Wang, J.R. Durig, Spectrochim. Acta 49A (1993) 2007–2026.
[29] J. Baker, A.A. Jarzecki, P. Pulay, J. Phys. Chem. 102A (1998) 1412.
[30] G. Rauhut, P. Pulay, J. Phys. Chem. 99 (1995) 3093.
[31] G. Fogarasi, P. Pulay, in: J.R. Durig (Ed.), Vibrational Spectra and Structure, vol. 14, Elsevier, Amsterdam, 1985.
[32] G. Fogarasi, X. Zhou, P.W. Taylor, P. Pulay, J. Am. Chem. Soc. 114 (1992) 8191.
[33] (a) T. Sundius, Vibr. Spectrosc. 29 (2002) 89;
(b) T. Sundius, J. Mol. Struct. 218 (1990) 321.
[34] S. Gunasekaran, S.R. Varadhan, K. Manoharan, Ind. J. Phys. 67B (1993) 95.
[35] A. Teimouri, A.N. Chermahini, K. Taban, H.A. Dabbagh, Spectrochim. Acta A 72 (2009) 369–377.
[36] R. Ustabas_, N. Suleymanoğlu, H. Tanak, Y.B. Alpaslan, Y. Unver, K. Sancak, J. Mol. Struct. 984 (2010) 137–145.
[37] L.J. Bellamy, R.L. Williams, Spectrochim. Acta 9 (1957) 341.
[38] J. Swaminathan, M. Ramalingam, N. Sundaraganesan, Spectrochim. Acta A 71 (2009) 1776.
[39] J.P. Jesson, H.W. Thompson, Spectrochim. Acta 13 (1958) 217.
[40] R. Saxena, L.D. Kauedpal, G.N. Mathur, J. Polym. Sci. A: Polym. Chem. 40 (2002) 3559.
[41] N. Sundaraganesan, S. Kalaichelvan, Spectrochim. Acta A 71 (2008) 898.
[42] S. Subashchandrabose, Akhil R. Krishnan, H. Saleem, V. Thanikachalam, G. Manikandan, Yusuf Erdogdu, J. Mol. Struct. 981 (2010) 59–70.
[43] V. Krishnakumar, R.J. Xavier, Spectrochimica Acta A 60 (2004) 709.
[44] S. Gunasekaran, S. Seshadri, S. Muthu, Indian J. Pure Appl. Phys. 44 (2006) 360.
[45] G. Varsanyi, Vibrational Spectra of Seven Hundred Benzene Derivatives, Academic Press, New York, 1969.
[46] G. Socrates, Infrared and Raman Characteristic Group Frequencies, third ed., John Wiley & Sons Ltd., Chichester, 2001.
[47] V. Krishnakumar, R. John Xavier, Indian J. Pure Appl. Phys. 41 (2003) 95–99.
[48] S. Sebastian, N. Sundaraganesan, S. Manoharan, Spectrochim. Acta A 74 (2008) 312.
[49] N. Sundaraganesan, S. Kalaichelvan, C. Meganathan, B. Dominic Joshua, J.P. Cornard, Spectrochim. Acta A. 71 (2008) 898.
[50] R.R. Randle, D.H. Whiffen, Report on Molecular Spectroscopy Conference, Institute of Petroleum, London, 1954.
[51] L.J. Bellamy, The Infrared Spectra of Complex Molecules, second ed., John Wiley, New York, 1959. pp. 203.

[52] G. Varsanyi, Vibrational Spectra of Seven Hundred benzene Derivatives, Academic Press, New York, 1969.
[53] S. Subashchandrabose, Akhil R. Krishnan, H. Saleem, R. Parameswaria, N. Sundaraganesan, V. Thanikachalam, G. Manikandan, Spectrochimica Acta A 77 (2010) 877–884.
[54] M. Snehalatha, C. Ravikumar, I.H. Joe, N. Sekar, V.S. Jayakumar, Spectrochim. Acta A 72 (2009) 654–662.
[55] M. Szafram, A. Komasa, E.B. Adamska, J. Mol. Struct. 827 (2007) 101–107.
[56] A.E. Reed, P.V.R. Schleye, Inorg. Chem. 27 (1988) 3969–3987.
[57] R.J. Xavier, E. Gobinath, Spectrochim. Acta A 91 (2012) 248–255.
[58] I. Fleming, Frontier Orbitals and Organic Chemical Reactions, John Wiley and Sons, New York, 1976. pp. 5–27.
[59] M.D. Diener, J.M. Alford, Nature 393 (1998) 668–671.
[60] H.O. Kalinowski, S. Berger, S. Braun, Carbon-13 NMR spectroscopy, John Wiley and Sons, Chichester, 1988.
[61] K. Pihlaja, E. Kleinpeter, Carbon-13 Chemical Shifts in Structural and Stero Chemical Analysis, VCH Publishers, Deerfield Beach, 1994.
[62] P.J. Garratt, in: A.R. Katritzky, C.W. Rees, E.F.V. Scriven (Eds.), Comprehensive Heterocyclic Chemistry II, vol. 4, Elsevier Science, 1996, pp. 127–163.